Time Resolved Photoluminescence Study on Silicon Nitride/Silicon-Rich-Oxide Superlattices Grown by Using Ion-Beam Sputtering Deposition

Kyu Man Cha, Young Dae Kim, Jung Hyun Kang, Jae-Yel Yi, Hong Jun Bark, Tae Hun Chung and Yong Kim*

Department of Physics, Dong-A University, Busan 604-714

Silicon nitride/silicon-rich-oxide (SiN/SRO) superlattices were fabricated by using dual ion-beam sputtering deposition. The effect of the SiN/SRO interface on the optical properties of the Si nanocrystals precipitated in the SRO layers was investigated by means of time-resolved photoluminescence measurements. The decay times of the photoluminescence for all superlattices were in the range of 20 ns $\sim$ 160 ns. Such small decay times reflect the strong effect of the non-radiative recombination centers existing at the SiN/SRO interfaces. For superlattices with thinner SRO thicknesses, the decay times were smaller for all detection wavelengths due to the increasing effect of the non-radiative recombination centers.

I. INTRODUCTION

Ultra-large-scale integrated-circuit (ULSI) technology has developed rapidly, and the minimum transistor gate length has reached the 100 nm level [1]. In contrast to the reduced dimension of ULSI device elements, the total length of the metal interconnections has increased significantly, with the expected line length being over 20 km in 2010. Such long interconnection lines cause several serious problems, most notably Joule heating and signal delay. Though new interconnection materials with low resistivities have been developed [2], signal delay remains an unsolved problem. It has been suggested that optical interconnects may provide the only viable solution [3].

Silicon is a naturally abundant element and has sufficient material strength to endure complicated ULSI process steps. However, silicon's pre-eminence in high-speed digital electronics does not generally extend to optoelectronics where the demand is for devices that can generate, guide, detect, and process optical signals. Almost all of the necessary Si-based photonic elements are now commercially available with the exception of an efficient, integratable light-emitting device. This final element is difficult to achieve because bulk silicon has an indirect bandgap, and radiative processes are relatively inefficient.

The quest for a silicon-based light source received a major boost with the discovery of efficient light emission from porous and nanocrystalline silicon, an effect that arises as a consequence of their nanoscale structures [4]. Indeed, devices based on porous silicon have been reported with external quantum efficiencies of over 1 % (commercially viable) [5]. However, porous silicon, which is a sponge-like substance, is mechanically fragile and has severe aging problems due to its high surface reactivity. Si nanocrystals embedded in a silica matrix also exhibit efficient room-temperature luminescence and offer an attractive alternative to porous silicon for device fabrication due to their stability and compatibility with standard ULSI processes. Si nanocrystals can be precipitated from substoichiometric silica films during high-temperature annealing. Relatively efficient photoluminescence is observed from the nanocrystals, and the emission wavelength depends on the nanocrystal size, enabling a degree of tunability [6]. Pulsed operation of a light-emitting diode (LED) with Si nanocrystals for over 100 hours without any noticeable aging effect has been demonstrated [7]. However, the external quantum efficiency is almost two orders of magnitude lower than that of porous silicon LEDs. This low efficiency stems from the difficulty of current injection to the nanocrystals due to the high barrier height of SiO_2 ($\sim$9 eV). The current is injected by Fowler-Nordheim tunneling or direct tunneling. Other non-radiative recombination paths also reduce the external quantum efficiency. These effects lead to early failure of LEDs due to overheating or oxide breakdown.

Previous device structures have employed Si nanocrystals randomly dispersed in a silica matrix. In addition,

the nanocrystal size dispersion has been significant. One way to circumvent this dispersion is to employ an amorphous superlattice for nanocrystal formation. The size dispersion of the Si nanocrystals after high-temperature annealing is reduced in such structures, and the tunneling distance is solely determined by the barrier-layer thickness [8]. These two effects increase the efficiency of current injection to the nanocrystals. In addition, the active optical volume can be increased simply by increasing the number of superlattice periods.

Further improvement of Si-based LEDs might be achieved by replacing large-bandgap SiO_2 with Si_3N_4 ($\sim$4.6 eV) or SiN_x. The barriers at the Si-Si_3N_4 interface are 2.0 eV and 1.5 eV for electrons and holes, respectively [9]. Thus, the lowered barriers will have a significant effect on increasing the current-injection efficiency. Furthermore, the field strength of 2 – 4 MV/cm required for bipolar injection is far lower than the breakdown field strength of Si_3N_4. Silicon nitride contains a high density of electron and hole traps. The high trap density has a positive effect on increasing the current injection efficiency. However, some of the traps may act as non-radiative recombination centers.

Therefore, silicon nitride/silicon rich oxide (SiN/SRO) superlattice structure may be ideal for an active layer in a highly efficient Si-based LED. Before this structure can be employed as an active layer in devices, systematic investigation of the optical properties for this structure will be required. In this research, we grew SiN/SRO superlattices by using dual ion-beam sputtering deposition, and we investigated their optical properties by using time-resolved photoluminescence.

II. EXPERIMENTAL DETAILS

SiN/SRO superlattices were deposited by employing a dual ion-beam sputtering (DIBS) deposition system. The detailed system configuration has reported elsewhere [10]. The sputtering target was a silicon wafer (resistivity $\sim$ 100 Ωcm), and the operating pressure was 4.4×10^{-4} Torr. For SRO growth, the beam energy and current of the primary Ar ion source were 750 eV and 7 mA, respectively. O_2 gas with a partial pressure of 8×10^{-6} Torr was introduced. Growth times were varied from 5 min to 15 min. For SiN growth, the beam energy and current of the primary Ar ion source were 750 eV and 7 mA, respectively. The beam energy and current of assisting N_2 ion source were 100 eV and 6 mA. The growth time was kept at 4 min. No intentional heating was applied to the substrate during deposition. Three SiN/SRO superlattices with 20 periods were prepared. The thickness of the SiN layer was kept at 4 nm, but the SRO thicknesses were 4, 6, and 12 nm. The samples were further annealed at 1100 °C for 2 h in N_2 gas.

Time-resolved photoluminescence (TRPL) was excited by using a pulsed N_2 laser (Laser Science VSL-337, 337.1-nm wavelength, 4-ns pulse width) with a repetition rate of 10 Hz. The PL was dispersed by using a 0.5-m monochromator (Dongwoo Optron DM500). The PL signal was detected with a cooled large-area Si avalanche photodiode (Advanced Photonix LAAPD module) with a 100-MHz digital oscilloscope. Continuous wave (CW) PL was excited by using a 488-nm Ar$^+$ ion laser (30 mW and 1-mm beam diameter) mechanically chopped at a frequency of 500 Hz. The PL signal was detected with a photomultiplier tube (Hamamatsu R928) by using a standard lock-in technique (Stanford Research SR810). All measurements were made at room temperature. The cross-sectional transmission electron microscope (TEM) image was observed by using JEOL JEM-2010 equipment through a standard preparation technique. The bonding configurations in the matrix of the samples were measured by using Fourier-Transform infrared spectroscopy (FTIR, Biorad Excalibur FTS-3000).

III. RESULTS AND DISCUSSION

Figure 1(a) shows a low-magnification cross-sectional TEM image of the SiN (4 nm)/ SRO (12 nm) superlattice sample. Except for a few layers close to the Si substrate, the individual layer thicknesses are fairly uniform, manifesting successful growth of the SiN/SRO superlattice structure. Figure 2(b) shows a high-resolution
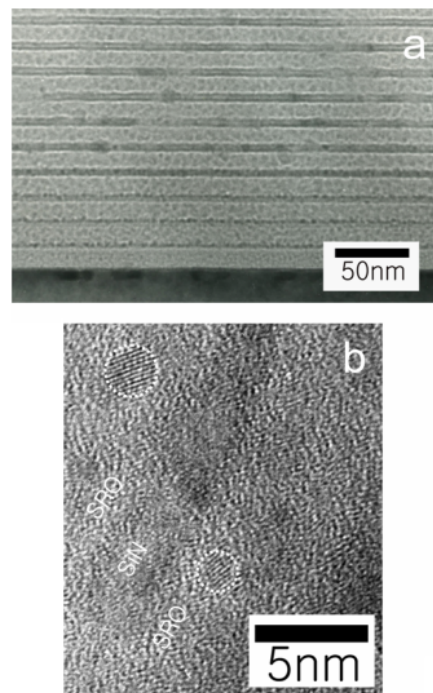
Fig. 1. (a) Low magnification TEM image of the SiN(4 nm)/SRO (12 nm) superlattice, (b) high-resolution TEM image near the SiN/SRO interface. Two- to three-nm-diameter Si nanocrystals are visible in the SRO layers.
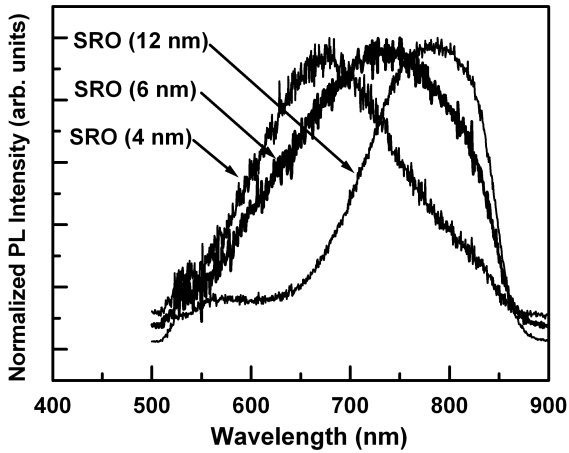
Fig. 2. CW PL spectra of superlattice samples with various SRO thicknesses.

Fig. 3. PL decays at various detection wavelengths for the SiN (4 nm)/SRO (6 nm) superlattice.

Fig. 4. PL decays detected at 730 nm from superlattice samples with various SRO layer thicknesses.

TEM image, and 2- to 3-nm-diameter Si nanocrystals are visible in the SRO layer. From FTIR observations, no hydrogen-related vibrations were observed for any sample. Therefore, effects related to hydrogen bonding need not be considered in present investigation. The respective nominal compositions of SRO and SiN layers were $SiO_{1.02}$ and $SiN_{0.6}$ from the FTIR analysis.

Before annealing, no significant PL was observed for any samples. Although there has been a report of the intense PL from an unannealed SiN layer. The PL was attributed to Si quantum dots formed by compositional fluctuation in the SiN matrix [11]. Since the samples were grown by using plasma-enhanced chemical vapor deposition, they contained large amounts of hydrogen, which could play a role in passivating non-radiative recombination centers. However, in our samples, there was no available hydrogen, as confirmed by the FTIR study. This may explain the lack of a PL signal even from the SiN layers. However, after annealing, all samples exhibited appreciable PL. Figure 2 shows the CW PL spectra for all superlattice samples. The PL spectra show a blue shift with decreasing SRO layer thickness due to the quantum confinement effect. The PLs are from Si nanocrystals precipitated in SRO layers, as observed in TEM image (Figure 1(b)), after high temperature annealing because a thick SiN single layer grown under the same conditions as the superlattice sample exhibits no appreciable PL after annealing.

Figure 3 shows representative TRPL spectra with a detection range from 550 nm to 900 nm for the SiN (4 nm)/SRO (6 nm) superlattice sample. In Figure 3, peak PL intensity at 0 delay time shows a maximum at a 670-nm wavelength. The decay time, τ, increases with increasing detection wavelength to an 800-nm wavelength and decreases again. Figure 4 displays the time decays of the PL from all sample at 730 nm. The decay time increases with increasing SRO layer thickness. Those time decays could be fitted with the well-known stretched ex-

ponential decay line shape [12]:
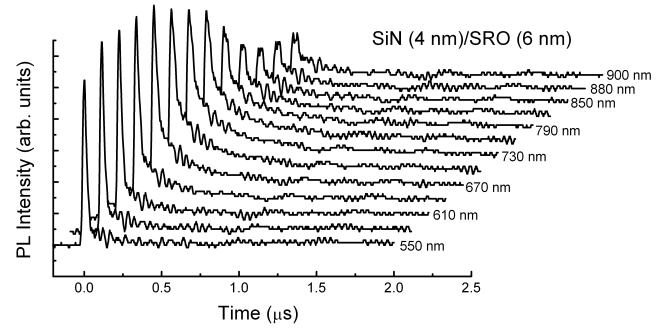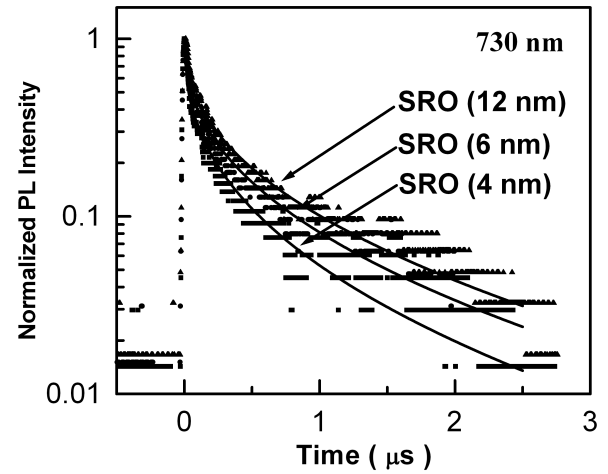
$$I(t) = I_0[\exp(-t/\tau)^\beta], \qquad (1)$$

where $I(t)$ and I_0 are the PL intensities at times t and 0 , respectively. τ is the characteristic decay time and reflects both the radiative and the non-radiative recombination times:

$$\tau^{-1} = \tau_R^{-1} + \tau_{NR}^{-1}, \qquad (2)$$

where τ_R and τ_{NR} are the radiative and the non-radiative recombination lifetimes, respectively. The dispersion factor, β, arises from communication between nanocrystals during the recombination process. As observed in Figure 4, the PL decay phenomena are well explained in term of a stretched exponential decay.

Figure 5 shows the variation of τ and β, evaluated from the fitting procedure shown in Figure 4, for all samples within the wavelength range from 550 nm to 900 nm. In the case of a thick SRO single layer, the precipitated Si nanocrystals are statistically distributed with various sizes, so the ensemble of Si nanocrystals exhibits a broad PL spectrum. When the separation between nanocrystals is sufficiently small to allow communication between
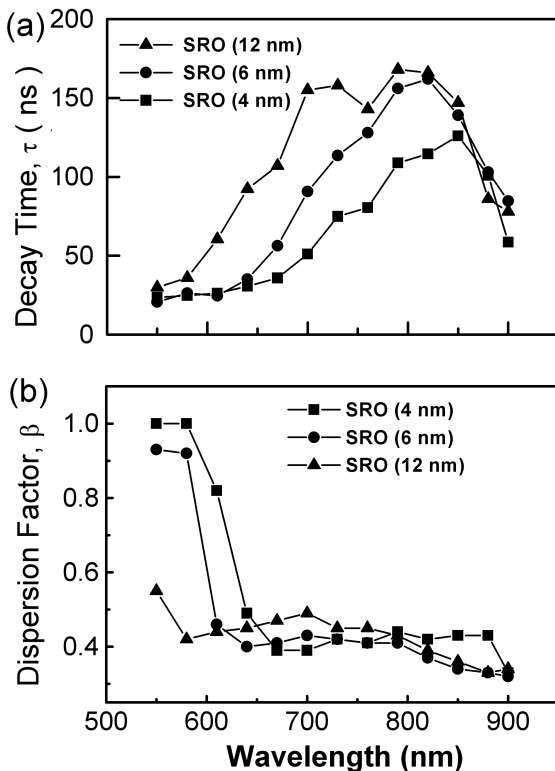
Fig. 5. (a) Decay time, τ, and (b) dispersion factor, β, as functions of the detection wavelength.

nanocrystals, e-h pairs generated from smaller nanocrystals, which have higher-energy ground states due to the quantum confinement effect, are efficiently transferred to larger nanocrystals and then recombine radiatively. A multiple transfer process can occur between adjacent nanocrystals before recombination. In this case, all different transfer paths have different characteristic transfer times and these times are included in the apparent PL decay time. Therefore, PL decay follows an extended exponential decay rather than a single exponential decay. In addition, this effect results in an increase of τ and a decrease of β with increasing detection wavelength because larger nanocrystals will have more complicated transfer processes [13].

This multiple transfer process also explains our general trend of the decay time variation in Figure 5. τ increases from 20 ns to 160 ns with increasing detection wavelength from 550 nm to 820 nm. The decrease of τ for detection wavelengths greater than 820 nm may be due to the generation of defects inside large nanocrystals. β is close to 1 at a detection wavelength of 550 nm for the SiN(4nm)/SRO(4 nm) and the SiN (4 nm)/SRO (6 nm) superlattices, indicating single exponential decay, and decreases rapidly with increasing detection wavelength. From 650 nm to 900 nm, β is around 0.4 for all samples. The decay time, τ, has been reported to be in the range from $\sim$1 μs to $\sim$100 μs, depending on the sample preparation conditions [14]. However, in our

samples, τ is within the range of 20 ns $\sim$ 160 ns, at least an order of magnitude smaller than the reported values. Such a small τ is due to the decrease of τ_{NR} due to the non-radiative recombination centers existing at the SiN/SRO interface. Obviously, the onset of the decay time increase is delayed toward larger detection wavelengths with decreasing SRO layer thickness. As the SRO layer thickness decreases, the average separation between nanocrystals and the SiN/SRO interface decreases; thus, τ decreases due to the increasing effect of non-radiative recombination centers. This effect causes such a delayed onset. For smaller nanocrystals, the effect of non-radiative recombination is more significant because of the increased surface/volume ratio of the smaller nanocrystals. Therefore, when non-radiative recombination centers are close to smaller nanocrystals, e-h pairs rapidly recombine via non-radiative recombination channels rather than migrate to other larger neighboring nanocrystals. In this case, the decay time will be described by a single exponential decay curve (*i.e.*, $\beta =$ 1) as observed in Figure 5(b).

IV. CONCLUSIONS

We have successfully fabricated SiN/SRO superlattices by using dual ion-beam sputtering deposition. The optical properties of the superlattices have been investigated by using time-resolved photoluminescence. The decay times were in the range of 20 ns $\sim$ 150 ns, an order of magnitude smaller than previously reported values. Such small decay times are attributed to the effect of non-recombination centers at the SiN/SRO boundary. In addition, we observed a decrease in the decay time with decreasing SRO thickness. This is due to the increasing effect of non-radiative channels as the average separation between nanocrystals and the SiN/SRO interface decreases.

REFERENCES

[1] International Technology Roadmap for Semiconductors (http://public.itrs.net)
[2] C. Y. Chang and S. M. Sze, *ULSI Ttechnology* (McGraw-Hill, New York, 1996).
[3] L. Pavesi, Materials Today **8**, 18 (2005).
[4] K. S. Min, Ph. D. Dissertation, Caltech, 2000.

[5] K. D. Hirschman, Ph. D. Dissertation, U. Rochester, 2000.

[6] S. H. Hong, S. Kim, S-H. Choi, K. J. Lee, H. Lee, K. J. Kim and D. W. Moon, J. Korean Phys. Soc. **45**, 116 (2004).

[7] N. Lalic, Ph. D. Dissertation, Royal Institute of Technology, 2000.

[8] M. Zacharias, J. Heitmann, R. Scholz, U. Kahler, M. Schmidt and J. Blasing, Appl. Phys. Lett. **80**, 661 (2002).

[9] V. A. Gritsenko, K. S. Zhuravlev, A. D. Milov, H. Wong, R. W. M. Kwok and J. B. Xu, Thin Solid Films **353**, 20 (1999).

[10] J. K. Kim, K. M. Cha, J. H. Kang, Y. D. Kim, Y. Kim, H. J. Bark, J-Y. Yi and T. H. Chung, J. Korean Phys. Soc. **45**, 728 (2004).

[11] N. M. Park, C. J. Choi, T. Y. Seong and S. J. Park, Phys. Rev. Lett. **86**, 1355 (2001).

[12] J. Linnros, N. Lalic, A. Galeckas and V. Grivickas, J. Appl. Phys. **86**, 6128 (1999).

[13] V. Vinciguerra, G. Franzo, F. Priolo, F. Iacona and S. Spinella, J. Appl. Phys. **87**, 8165 (2000).

[14] A. R. Wilkinson and R. G. Elliman, Phys. Rev. B **68**, 155302 (2003).